J Nanopart Res (2021) 23: 152
https://doi.org/10.1007/s11051-021-05238-w

RESEARCH PAPER

Unraveling reaction pathways for tuning bimetallic nanoparticle structures: role of reactant addition sequence

Krishna V. Kinhal · Nirav Bhatt · S. Pushpavanam

Received: 12 October 2020 / Accepted: 9 May 2021 / Published online: 23 July 2021

Abstract In this work, we experimentally demonstrate the synthesis of different bimetallic Ag–Cu nanostructures like core–shell, Janus particles. It is shown that different nanoparticle structures are associated with different reaction pathways. The pathway is manipulated by modifying the operating conditions (reactant sequence in this case) of the reactions. Ascorbic acid and cetyltrimethylammonium bromide (CTAB) is used as the reducing agent and the capping agent, respectively. Silver nitrate and copper nitrate are used as precursors. The reaction is carried out under microwave-assisted heating, which intensifies metal ion reduction. Two protocols are studied: (I) sequential and (II) simultaneous addition of precursors. By changing the sequence of the precursor addition, the morphology of the bimetallic nanoparticles was altered. Janus particles of size 25–30 nm were formed under the simultaneous addition and the sequential addition when the silver precursor is added first, followed by the copper precursor. When the sequence of precursor addition was reversed, i.e., copper precursor followed by silver, Cu core-Ag shell particles of size 65 nm were formed. We propose mechanisms that help understand the formation of these different structures. Resistance to oxidation studies showed that the particles with Cu core-Ag shell morphology were more resistant to oxidation than Janus particles.

Keywords Bimetallic nanoparticles · Microwave synthesis · Precursor sequence · Janus particles · Core–shell particles

K. V. Kinhal · S. Pushpavanam (✉)
Department of Chemical Engineering, Indian Institute of Technology Madras, Chennai 600036, India
e-mail: spush@iitm.ac.in

N. Bhatt (✉)
Department of Biotechnology, Indian Institute of Technology Madras, Chennai 600036, India
e-mail: niravbhatt@iitm.ac.in

Introduction

The essence of any chemical reaction is the conversion of reactants into the desired product. These may involve several complex intermediate steps and mechanisms. In these systems, different reaction pathways can give rise to different products starting from the same reactants. These reaction pathways are sensitive to reaction conditions; as a result, different pathways generate varied products under different reaction conditions. This strategy has been applied in various organic, catalytic, and biological reactions to obtain varied products in a single process ((Ney and Wolfe 2005; Kushida et al. 2017)). However, the idea of exploiting multiple pathways in a single process has not been explored in nanoparticle synthesis. In this

work, we show how this perspective can be extended to the synthesis of metallic nanoparticles.

Metallic nanoparticles have a wide range of applications. In the medical field, they serve as drug delivery agents (Cheng et al. 2010), in wastewater treatment as an anti-bacterial agent (Zhang et al. 2013), and in chemical process industries as a catalyst (Cuenya 2010). Nanoparticles of precious metals such as gold and silver have been widely studied for these applications, but they can be prohibitively expensive. Copper nanoparticles are an attractive alternative to gold and silver. However, they are oxidized easily by air or dissolved oxygen in the water (Gawande et al. 2016; Pacioni et al. 2013; Yabuki and Tanaka 2011).

In this context, bimetallic nanoparticles have gained much interest in recent times as they offer an alternative to expensive noble metallic nanoparticles and unstable transition metallic nanoparticles. These nanoparticles, made of a mixture of metals, can exhibit different morphologies like core–shell, Janus particles, and mixed alloys. The morphologies are determined by the properties (atomic radius, bond strength, surface energy) of the two individual metals, which constitute the bimetallic nanoparticles (Ferrando et al. 2008).

A standard method to synthesize bimetallic nanoparticles is through the chemical reduction of precursors. This method provides good control over the shape and size of nanoparticles. To develop a green process, several earlier studies have focused on the use of environmentally friendly reducing agents such as ascorbic acid. Nanoparticle synthesis using these eco-friendly reagents requires a high temperature for the reduction of transition metals, as they are weak reducing agents. The reduction can be carried out using a conventional heating apparatus such as an oil bath (Nadagouda et al. 2007; Panigrahi et al. 2005; Tsuji et al. 2009). These heating methods result in a non-uniform temperature distribution inside the reactor and result in a broad nanoparticle size distribution (Schanche 2003). To overcome the problem of non-uniform temperature distribution, microwaves have been alternatively used for heating (Cai et al. 2017).

Synthesis of the nanoparticles using microwave heating and its effect on intensifying the reaction process have been studied widely (Horikoshi and Serpone 2013). It is known that microwave heating enhances the reaction rates of chemical processes by decreasing the activation energy of the molecules (Zhou et al. 2016). Moreover, heating through the microwave provides a uniform temperature and speeds up the nucleation process via an instantaneous temperature rise (Horikoshi et al. 2010). Valodkar et al. (2011) synthesized Cu-Ag nanoparticles using ascorbic acid as a reducing agent. They considered the effect of copper concentration on the localized surface plasmon resonance (LSPR) peak of the nanoparticles. Tsuji et al. (Tsuji et al. 2010) investigated the mechanism of the formation of silver copper bimetallic nanoparticles. They synthesized particles with silver at the core and copper at the shell and vice versa by changing the concentration of seeds and precursors. However, computational studies show that the Cu core-Ag shell formations are thermodynamically favorable and stable compared to Ag core-Cu shell formations (Ferrando et al. 2008; Rossi et al. 2004). Studies performed by Ferrando (2015) discussed different computational and experimental results in the transition of nanoparticle structures by modifying the atomic content of the two metals involved. However, the transition between different nanoparticle structures by modifying operating conditions at a constant atomic content has not been addressed yet.

Bimetallic nanoparticles with different structures have been widely studied (Langlois et al. 2012; Miyakawa et al. 2014). Core–shell and Janus structures are two of the most common morphologies that exist for the bimetallic system. The synthesis of Janus bimetallic nanoparticles so far has been carried out via complex processes such as interfacial galvanic exchange reactions (Song et al. 2012), interfacial etching of core–shell particles (Chen et al. 2016), or by physical methods (Langlois et al. 2012). For the synthesis of core–shell structures, the process of seed mediation has been widely used (Ma et al. 2010; Wang et al. 2016; Lu et al. 2002; Mandal et al. 2003). It is hypothesized that the metal salt (primary) that gets reduced first forms the core structure, and the component (secondary metal salt) added later forms the shell around the previously synthesized core nanoparticles. This holds true when the two metals involved have a comparable atomic radius and surface energies (e.g., Au, Ag). However, this mechanism cannot be assumed for the bimetallic nanoparticles made of elements with different atomic radius and surface energies (e.g., Ag, Cu).

In the context of bimetallic nanoparticles, in light of the above studies, it is clear that the different structures are formed by different reaction pathways. The question arises as to whether it is possible to manipulate these pathways experimentally by controlling the operating conditions. This control can help in tuning the final product characteristics, i.e., the morphology of bimetallic nanoparticles.

In this work, we explore the possibility of obtaining different structures like core–shell and Janus particles by changing the process conditions. The focus is on the importance of the reactant sequence in manipulating the reaction pathways and thereby tune the morphology of bimetallic nanoparticles. The transition-noble bimetallic nanoparticle system of copper and silver is chosen as an example to understand the effect of the precursor sequence as both metal ions can be reduced by a single reducing agent. Moreover, copper and silver exhibit localized surface plasmon resonance (LSPR) properties at nanoscale in the visible region, which makes it easier to characterize the formation of bimetallic nanoparticles through UV–vis spectroscopy. It is shown, in this work, that by varying the sequence of addition of precursors and modifying the reaction pathway, different morphologies like core–shell and Janus nanoparticles can be tuned McIntyre and Cook 1975. Studies on resistance to oxidation were performed to understand the stability of these structures. It is further shown, for the first time, that Janus bimetallic nanoparticles can be synthesized through a simple microwave-assisted chemical reduction method.

Experimental procedure

Materials

For the experiments, copper nitrate trihydrate ($Cu(NO_3)_2.3H_2O$), silver nitrate ($AgNO_3$), ascorbic acid, and CTAB were purchased from Merck India Pvt. Ltd., Mumbai, India. Deionized water was obtained from the Evoqua Millipore® system. Carbon-coated nickel TEM grids were obtained from Tadpella Inc., USA, for performing TEM imaging of nanoparticles.

Synthesis of nanoparticles

Stock solutions of 0.01 M of $Cu(NO_3)_2{\cdot}3H_2O$ and 0.01 M $AgNO_3$ solutions were prepared. These serve as precursors for the Cu and Ag nanoparticles, respectively. 0.5 M ascorbic acid solution was used as a reducing agent in all the experiments. CTAB is employed as a capping agent and a phase-directing agent.

Three different sets of experiments were carried out systematically to vary the pathways for the formation of different nanoparticle morphologies. The reaction pathway was altered by changing the sequence of precursor addition in batch synthesis. In the first set of experiments, we analyze the formation of nanoparticles by changing the sequence of two precursors used for the synthesis, viz. copper nitrate and silver nitrate. We also examine what nanoparticle structures are formed if both the precursors are reduced simultaneously. Furthermore, we investigate the antioxidation properties of different bimetallic nanoparticles synthesized in this study. The experimental protocols are schematically described in Fig. 1. 100 ml of deionized water was poured into a 500-ml glass beaker. One milliliter of 0.5 M ascorbic acid solution was added to the beaker. Furthermore, 0.1 g of CTAB (capping agent) was added to this solution to prevent the agglomeration of the synthesized nanoparticles. Later, the first precursor ($AgNO_3$ in the experiment E1 and $Cu(NO_3)_2{\cdot}3H_2O$ in the experiment E2) solution was added to the CTAB and ascorbic acid mixture. The resulting solution was stirred vigorously for 1 min at 600 rpm. The initial pH of the solution was brought to 11 by dropwise addition of 1 M sodium hydroxide. This solution was subjected to 30 s of microwave heating (750 W, 2.45 GHz).

The formation of primary nanoparticles corresponding to the first precursor was confirmed by the development of color in the solution (yellow in experiment E1 and brown in experiment E2). UV–vis spectroscopy was performed to confirm the formation of the primary nanoparticles. Later, 1 ml of the second precursor ($Cu(NO_3)_2{\cdot}3H_2O$ in the experiment E1 and $AgNO_3$ in the experiment E2) was added dropwise to the solution while mixing it at 600 rpm. The resultant solution was further heated in a microwave for 30 s at 750 W. The solution turned reddish-brown (in E1) or

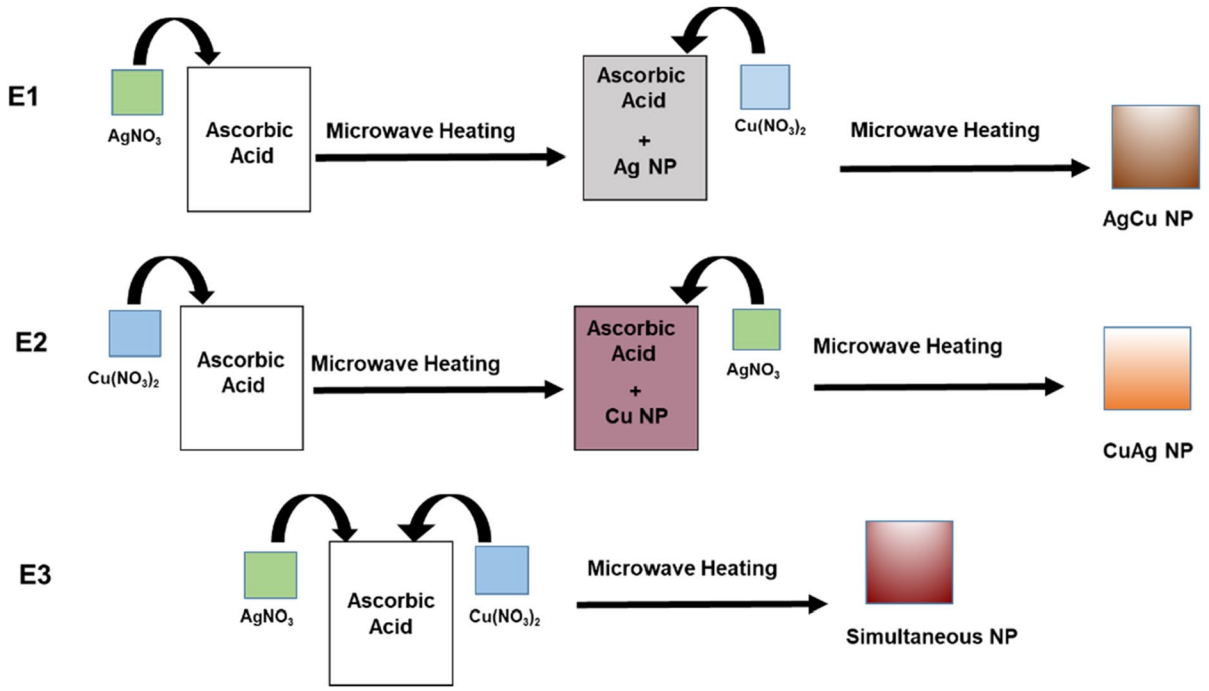

Fig. 1 Schematic of different experimental procedures for the synthesis of bimetallic nanoparticles. The sequence of precursor addition is altered in experiments E1 and E2. Precursors are added simultaneously in experiment E3

yellow (in E2), indicating the formation of bimetallic nanoparticles.

For experiment E3, initially, a 100 ml solution consisting of 0.1 g CTAB was prepared. Later, 1 ml of 0.01 M $Cu(NO_3)_2{\cdot}3H_2O$ and 1 ml of 0.01 M $AgNO_3$ were added at the same time. Later, 1 ml of 0.5 M ascorbic acid was added to the solution of the precursor mixture. The resulting solution was heated for 60 s in the microwave (750 W, 2.45 GHz). After heating, the solution turned dark red, indicating the formation of nanoparticles.

The solution containing nanoparticles was later analyzed through different characterization techniques.

Precautionary measures The synthesis of nanoparticles is extremely sensitive to the operating conditions. Hence, it is important to control these conditions as accurately as possible to obtain reproducible results. The precautionary measures taken are described next.

a) Temperature distribution in the system can alter the nucleation and cause polydispersity in nanoparticle size. It was challenging to measure the temperature of the solution during microwave heating. However, the temperature of the solution after the microwave heating process was measured to be 94° C. Therefore, the temperature of the solution after the microwave heating was maintained at 94° C through a hot oil bath until the experiment was complete.

b) Mixing plays a vital role in ensuring uniform nucleation of particles. It is necessary to have vigorous stirring during the addition of the reactants. Different stirrers may have different power ratings, which may lead to varying stirring speeds. Moreover, different stirring pellets may again lead to dissimilar mixing patterns. To keep the mixing conditions constant, all the experiments were conducted in the same stirrer (IKA® RCT Basic) and the same magnetic pellet. It was also ensured that the position of the pellet was always at the center of the reactor during the experiment. It was challenging to stir during microwave heating. Therefore, the stirring was employed before and after the microwave heating.

c) Impurities can contribute to the polydispersity of the nanoparticles by providing heterogeneous nucleation sites. Therefore, the glassware and stirring pallet used in the experiments were thoroughly washed using a Piranha solution (1:3 ratio of 30% H_2O_2 and H_2SO_4) and deionized water before every experiment.
d) Silver nitrate is sensitive to light and can undergo a reduction in the presence of light. This affects the synthesis of nanoparticles. Therefore, the reactions were carried out with all the lights switched off to eliminate the interference of light during nanoparticle synthesis.

Nanoparticle characterization

Initially, the nanoparticle solution was characterized using UV–vis spectroscopy (JASCO V-630). The metal nanoparticles interact with light and exhibit an LSPR. This is caused by the interaction of electrons present on the surface of metals and the electromagnetic field of emitted photons. The formation of nanoparticles can hence be confirmed from the absorption spectra. The peak in the spectrum indicates the formation of nanoparticles and is observed in the visible region of light for silver and copper nanoparticles in the wavelength range of 350 nm–450 nm, and 550 nm–650 nm, respectively.

Furthermore, the solution containing nanoparticles was centrifuged, and the residue was collected and dried. The dried powder containing nanoparticles was subjected to XRD (Rigaku Miniflex™) to determine the crystal structure of nanoparticles. The XRD data for pure silver and copper nanoparticles were analyzed, and the crystal planes corresponding to the peaks were calculated. The details of these data and computations are given in Supporting Information. X-ray photoelectron spectroscopy analysis (XPS) (using Thermo Fisher Scientific ESCALAB Xi+) was performed on bimetallic nanoparticles to analyze the surface elemental composition. Furthermore, SEM (using Hitachi S4000) and TEM (using JOEL 3010 and Tecnai™ T20) images were obtained and analyzed to determine and understand the morphology of the particles. Small-angle electron diffraction (SAED) was performed along with TEM imaging to understand the crystalline structure of nanoparticles. The surface elemental composition of the particles was confirmed by performing EDS (using Oxford Instruments). Particle size analysis was performed on the TEM image using ImageJ software provided by the National Institute of Health, USA. One hundred particles were considered for the particle size analysis, and the average Ferret's diameter was calculated. All the experiments were carried out three times to ensure reproducibility.

Results

Experiment E1 (Ag precursor followed by Cu precursor)

In this case, initially, silver nanoparticles are synthesized by the addition of $AgNO_3$ in an ascorbic acid solution. The UV–vis absorption spectra (Fig. 2a) confirm the presence of silver nanoparticles (dashed lines) as the LSPR peak is obtained at 409 nm. Later, when the copper precursor ($CuNO_3{\cdot}3H_2O$) was added to the solution, the UV–vis absorption data (continuous line) confirm the formation of copper nanoparticles through a weak LSPR peak at 580 nm. The presence of silver in the nanoparticles is confirmed through an LSPR peak at 401 nm. This spectrum is similar to the spectra of Ag–Cu Janus nanoparticles obtained in the literature (Pellarin et al. 2015). The XPS result shown in Fig. 2b indicates the presence of copper and silver at the nanoparticle surface. Peaks at 368 eV and 373 eV were attributed to the presence of silver. Furthermore, analysis was carried out by deconvoluting XPS data of the corresponding element at a higher resolution. This was performed to understand its oxidation state. The details of the analysis are discussed in Section S3 of the Supporting Information. High-resolution XPS (Figure S2a) reveals the presence of Ag and Ag_2O on the particle surface. The peak corresponding to copper could be observed at 932 eV. Detailed analysis (Figure S2b) indicates the contribution of CuO, Cu_2O to the copper peak. Besides, the O 1 s peak at 531 eV confirms the surface oxidation. Furthermore, analysis at high resolution (Figure S2c) indicates that oxygen is present in the form of oxides of copper and silicon. The presence of silicon in the XPS data is attributed to the silicon wafer, on which the nanoparticles were dried and analyzed. The XRD spectrum of the bimetallic nanoparticles in Fig. 2c is compared with the XRD

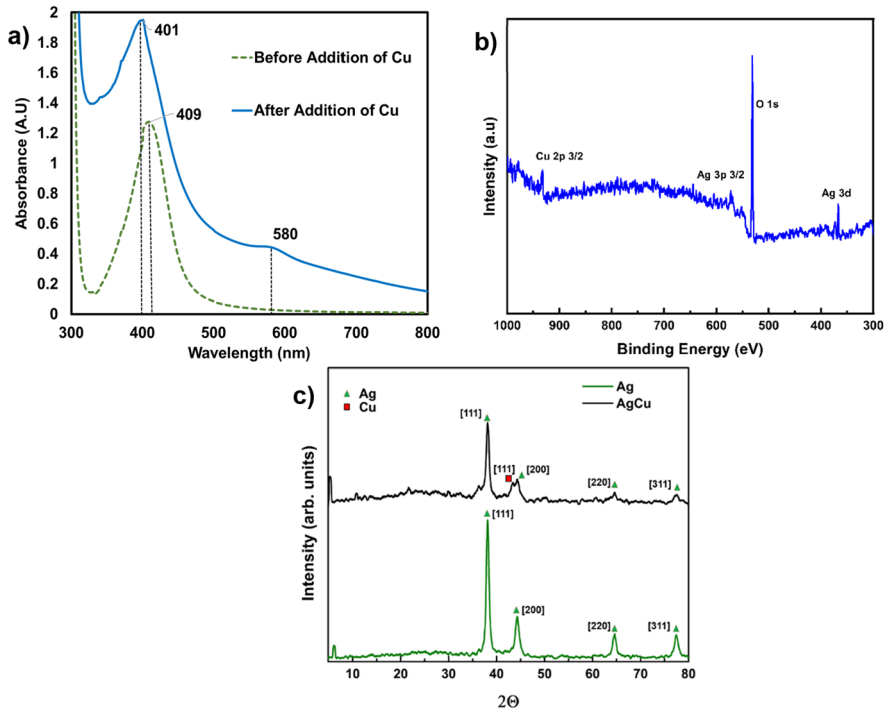

Fig. 2 **a**) UV–vis absorption spectra indicating LSPR peak for silver before the addition of copper precursor and peaks for copper and silver after addition of copper precursor, **b**) XPS spectrum confirms the presence of oxidized copper and silver on the nanoparticle surface, and **c**) XRD spectrum for the AgCu bimetallic nanoparticles, synthesized in experiment E1 with microwave heating

spectra of pure silver and copper nanoparticles (See Supporting Information). The analysis of the particles before the addition of the second precursor indicates the formation of silver nanoparticles with [111] (at 2Θ = 38.16), [200] (at 2Θ = 44.38), [220] (at 2Θ = 64.42), and [311] (at 2Θ = 77.44) crystal planes. Furthermore, the analysis of nanoparticles formed after the addition of the second precursor indicated the presence of [111] Cu planes (at 2Θ = 43.51) and [111] Ag plane (at 2Θ = 38.16) and [200] and [311] Ag planes at 2Θ = 44.36 and at 2Θ = 77.44 respectively. The TEM image Fig. 3a indicates the formation of the bimetallic nanoparticles with an average particle size of 23.5 nm. It can be observed that the particles have Janus morphology. The lighter portion of the particle in the TEM image corresponds to copper, whereas the darker portion corresponds to silver (see the inset of Fig. 3a). The contrast is obtained due to different atomic mass (and hence the densities) of silver (107.868 amu) and copper (63.546 amu). Since the contrast is consistent in all the particles (a darker portion is always at one side of the particle), the contrast due to the different thickness of the particles can be ruled out. The SAED pattern (Fig. 3b) analysis of the nanoparticles revealed the formation of Ag [111], [220], and [311] planes and Cu [111], [200], and [220] planes. These results are consistent with the XRD data. The details are discussed in Supporting Information Section S2. Spherical nanoparticles could be observed in the SEM image, included in the Supporting Information (Figure S6a). Furthermore, the elemental analysis in Fig. 3c confirms the presence of elemental copper and silver in the nanoparticles. The EDS spectrum (see Figure S7a in the Supporting Information) further indicates the presence of silver and copper on the particle surface.

Experiment E2 (Cu precursor followed by Ag precursor)

When the sequence of precursor addition is changed, copper nanoparticles are synthesized initially. The UV–vis absorption spectra in Fig. 4a (dash lines and inset) confirm the formation of copper nanoparticles as a weak LSPR peak corresponding to copper nanoparticles at 590 nm could be observed. Later, after the addition of the silver precursor, a dominant LSPR peak for Ag is formed at 431 nm, and the peak for copper diminishes. Since the LSPR is a surface phenomenon, the absence of a copper LSPR peak indicates the possibility of a core–shell formation with copper at the core and silver as a shell. We refer to

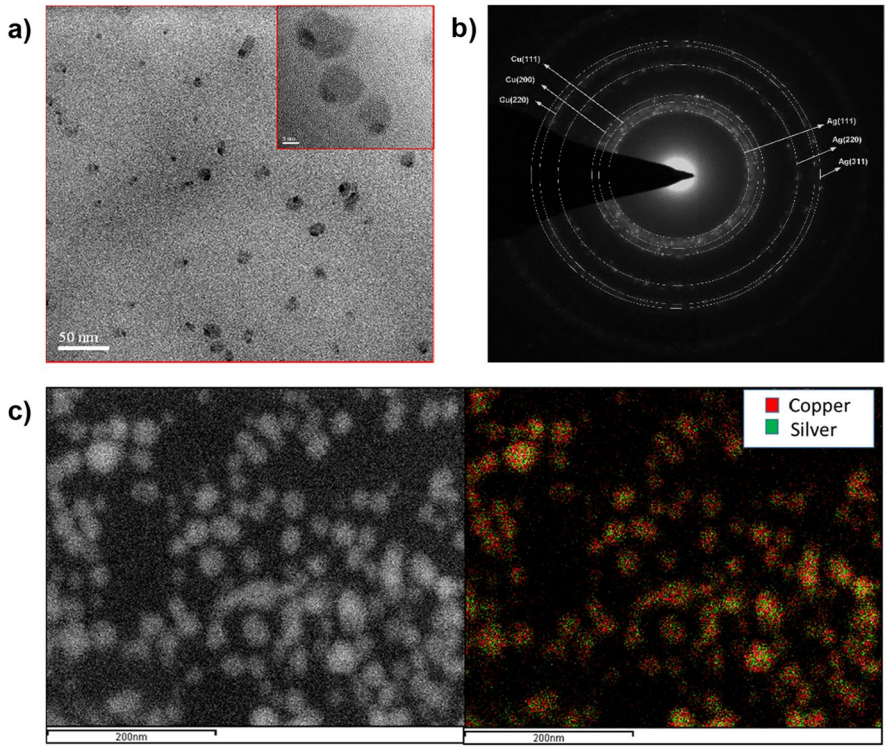

Fig. 3 **a**) TEM image of bimetallic nanoparticles indicating the formation of Janus particles with dark portion representing silver, whereas lighter portion representing copper, **b**) SAED pattern of the particles revealing their crystalline structure, and **c**) elemental analysis of the bimetallic nanoparticles synthesized in the experiment E1 showing the original image (left) and analyzed image (right) confirming the presence of copper and silver in the particles

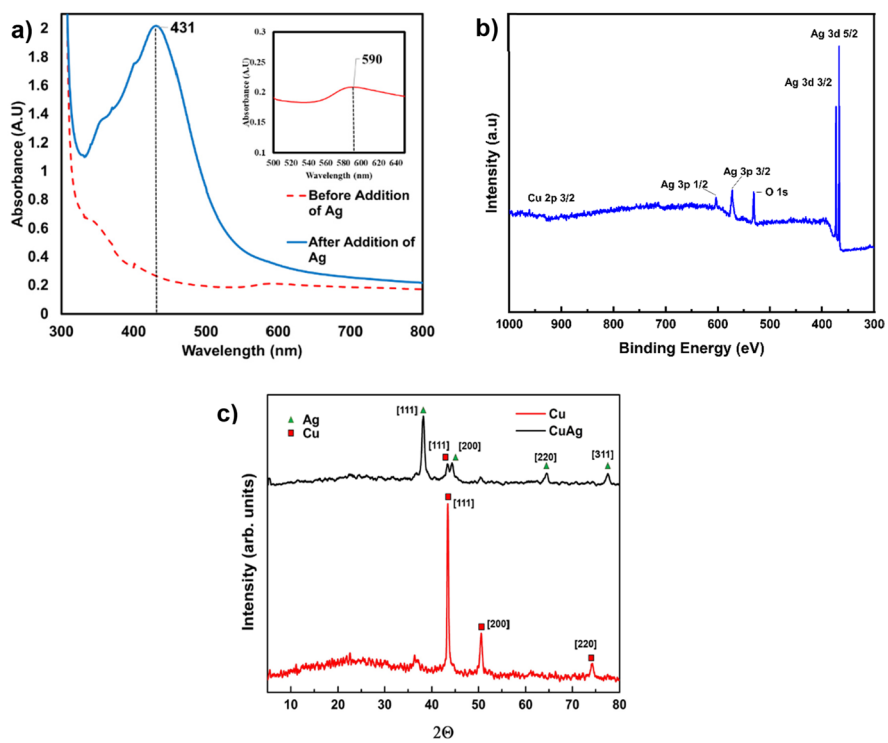

Fig. 4 Characterization of bimetallic nanoparticles synthesized in experiment E2 with microwave heating. **a**) UV–vis absorption spectra with the LSPR peak for copper nanoparticles formed before the addition of the second precursor is shown in the inset, **b**) XPS spectrum indicating presence of silver and oxygen on the nanoparticle surface, and **c**) XRD data for the Cu-Ag bimetallic nanoparticles

these particles as Cu-Ag particles. The XPS results (Fig. 4b) reveal the presence of silver on the surface. The high-intensity peaks at 367 eV and 373 eV correspond to silver. Deconvoluted high-resolution XPS (Figure S3a) further indicates the presence of Ag and Ag_2O on the nanoparticle surface. The low O 1 s peak at 531 eV implies minimal surface oxidation. The minor Cu (2p 3/2 orbital) peak at 932 eV was observed and can be attributed to fewer particles that did not form core–shell structures. The peak could also imply the formation of few copper nanoparticles that may form through the copper ions displaced during the galvanic reactions occurring at the surface. The deconvolution of O 1 s peak (Figure S3c) revealed contribution from oxides of silicon and copper. XRD pattern in Fig. 4c indicates the formation of copper particles initially with [111] ($2\Theta = 43.36$), [200] ($2\Theta = 50.44$), and [220] ($2\Theta = 74.43$) planes. After the addition of $AgNO_3$, the particles show the presence of [111] Ag ($2\Theta = 38.08$), [200] Ag ($2\Theta = 44.34$), [220] Ag ($2\Theta = 64.44$), and [311] Ag ($2\Theta = 77.50$), along with [111] Cu ($2\Theta = 43.28$) planes. The core–shell structure of the nanoparticles with an average size of 65 nm could be confirmed through the TEM image (Fig. 5a). The lighter part of the particles corresponds to copper, and the darker portion of the particle corresponds to silver (see inset image in Fig. 5a). The SAED pattern of the nanoparticles in Fig. 5b indicates the presence of Ag [111], [220], and [311] planes and Cu [111], [200], and [220] planes. These results are consistent with the structure obtained from XRD data. The SEM image (see Figure S6b in the Supporting Information) indicates that the particles formed are non-uniform in size. The elemental analysis of the particles in Fig. 5c confirms the presence of silver on the nanoparticle surface. The EDS spectrum is included as Figure S7b in the Supporting Information. Minor Cu peak in the EDS spectra further confirms the formation of core–shell structure.

Experiment E3 (simultaneous addition)

The UV–vis spectral data (Fig. 6a) obtained for the simultaneous addition of precursors are similar to the spectra obtained in experiment E1. A sharp LSPR peak for silver is obtained at 401 nm, and a broad copper LSPR peak can be seen at 576 nm. The XPS results (Fig. 6b) indicate the presence of copper and silver at the nanoparticle surface. Here, the silver

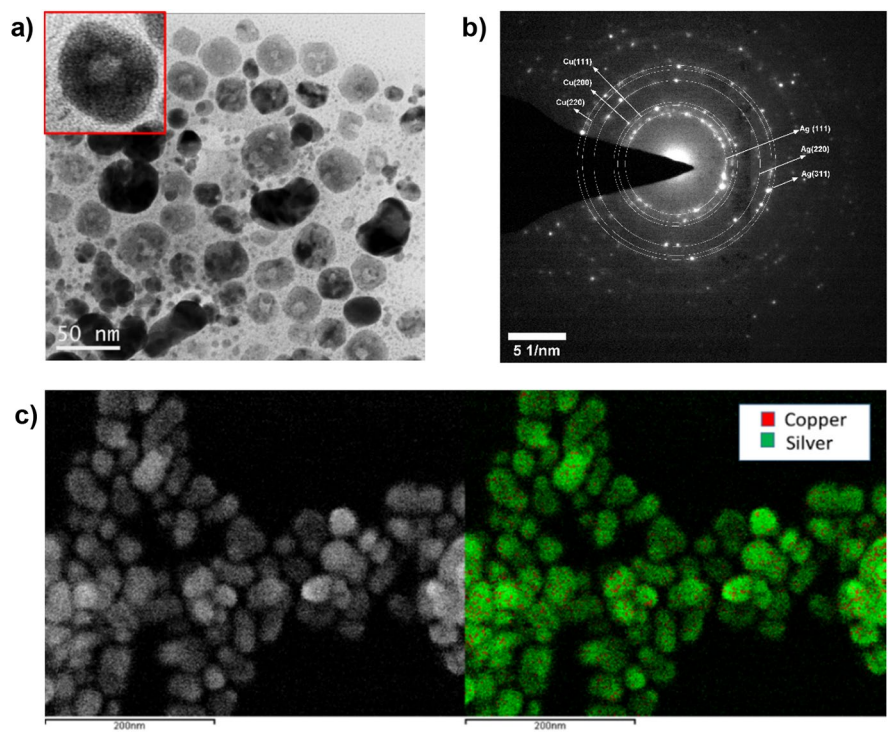

Fig. 5 **a**) TEM image of bimetallic nanoparticles indicating the formation of core–shell particles, **b**) SAED pattern of the bimetallic nanoparticles attributing different crystalline states, and **c**) elemental analysis of the bimetallic nanoparticles synthesized in experiment E2 with the original image (left) and analyzed image (right) confirming the presence of copper and silver in the particles

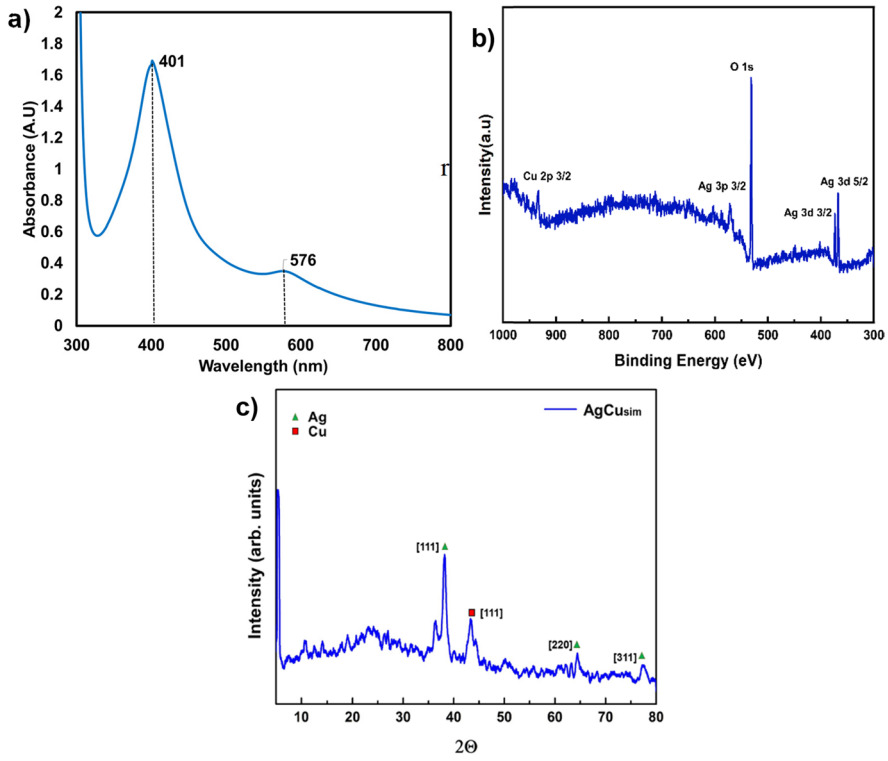

Fig. 6 **a**) UV–vis absorption spectra indicating the LSPR peaks corresponding to silver and copper, **b**) XPS data indicating the presence of silver and copper on the nanoparticle surface, and **c**) XRD spectrum analysis for the characterization of bimetallic nanoparticle synthesized in experiment E3 with microwave heating

peak is observed at 368 eV and 374 eV. These peaks were further analyzed and deconvoluted to understand the oxidation states. The deconvolution as performed in Supporting Information (Figure S4a) indicates the presence of silver in the form of Ag and Ag_2O. The peak corresponding to copper was observed at 933 eV. On further analysis of the copper peak by deconvolution (Figure S4b), it is observed that copper on the surface exists as CuO and Cu_2O. The high-intensity oxygen peak in the XPS spectra at 531 eV indicates surface oxidation. The analysis of the data at high resolution in Figure S4c implies that the oxygen peak is contributed by oxides of copper and silicon. The XRD pattern in Fig. 6c describes the formation of crystalline silver [111] planes ($2\Theta = 38.18$), [200] planes ($2\Theta = 44.34$), [220] planes ($2\Theta = 64.44$), and [311] planes ($2\Theta = 77.56$), and highly crystalline copper [111] planes ($2\Theta = 43.48$). The TEM image in Fig. 7a indicates the formation of a mixture of morphologies consisting of Janus, core–shell particles, along with copper particles with an average size of 33 nm, in this case. We refer to these particles as $AgCu_{Sim}$. The SAED pattern in Fig. 7b indicates the formation of Ag [111], [220] planes, and Cu [200] crystalline structure in the nanoparticles. It can be observed from the SEM image included as Figure S6c in the Supporting Information, the nanoparticles formed are comparatively smaller than those in experiment E2 (Cu followed by Ag) and similar to nanoparticles formed in experiment E1 (Ag followed by Cu). The elemental analysis in Fig. 7c confirms the presence of elemental copper and silver in the nanoparticles.

Anti-oxidation studies

It is well known that the copper nanoparticles oxidize rapidly and lose their surface activity (Pacioni et al. 2013). In comparison to Cu nanoparticles, Ag nanoparticles are less prone to oxidation. We now analyze the stability of different bimetallic nanoparticles obtained under different experimental conditions. This will help in the selection of the right sequence based on the applications. For instance, in conductive inks, the particles are required to be resistant to oxidation to achieve the desired conductivity. To understand the resistance of bimetallic nanoparticles to oxidation, the solution containing nanoparticles

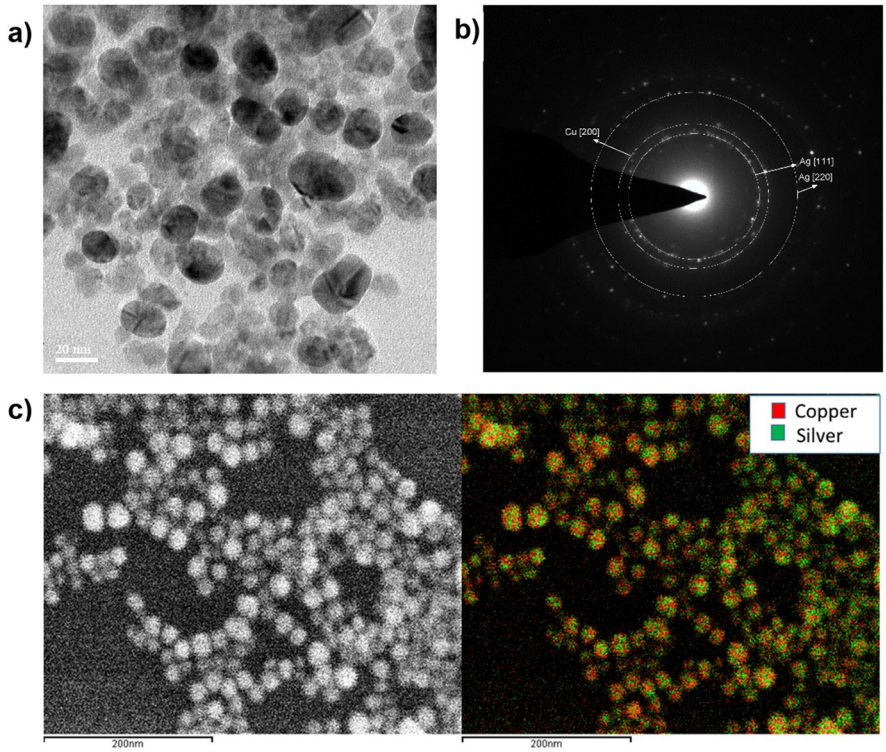

Fig. 7 **a**) TEM image of bimetallic nanoparticles synthesized in E3 shows the formation of a mixture of nanoparticle morphologies, **b**) SAED pattern of the nanoparticles indicating the crystalline structure, and **c**) elemental analysis of the nanoparticles synthesized in experiment E3, the original image (left), and analyzed image (right) confirming the presence of copper and silver in the particles are shown

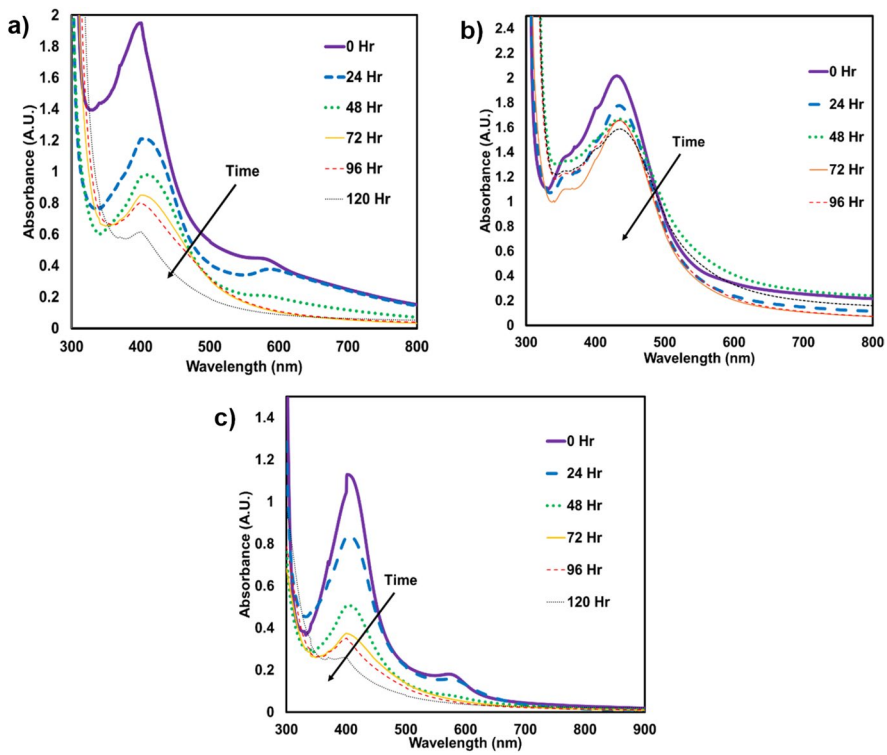

Fig. 8 UV–vis absorption spectra for three experiments: **a**) E1 (silver precursor followed by copper precursor), **b**) E2 (copper precursor followed by silver precursor), and **c**) E3 (simultaneous addition of precursors). Spectra for nanoparticles formed in E1 and E3 show degradation with time, whereas spectra for nanoparticles formed in E2 show minimal degradation with time

obtained from all three experiments was kept at ambient temperature (30 ± 2° C) for 120 h. The absorption spectrum and the images of the nanoparticle solution were obtained every 24 h. The spectrum and the color of the solution at different time instants are shown in Figs. 8 and 9, respectively. Figure 8a, b, and c show the UV–vis absorption spectra for the bimetallic nanoparticles obtained in the experiments E1, E2, and E3, respectively. The silver and copper LSPR peaks for the experiments E1 (Fig. 8a) and E3 (Fig. 8c) show significant degradation with time. This is attributed to the degradation of nanoparticles through oxidation. The absorption spectra observed for the bimetallic nanoparticle solution obtained in experiment E2 (Fig. 8b) degrade initially but at later instants shows stable LSPR peaks indicating stable nanoparticle solutions. It was observed that the red solution from the experiments E1 (AgCu) and E3 ($AgCu_{Sim}$) eventually turned yellowish (Fig. 9a and c) with time indicating oxidation of copper. The nanoparticle solution obtained in experiment E2 (Cu-Ag) retained the yellowish color (Fig. 9b), indicating the nanoparticles synthesized here are stable and resistant to oxidation. Comparing O 1 s peaks from the XPS data in Figs. 2b, 4b, and 6b further ascertains that nanoparticles formed in E1 and E3 are prone to

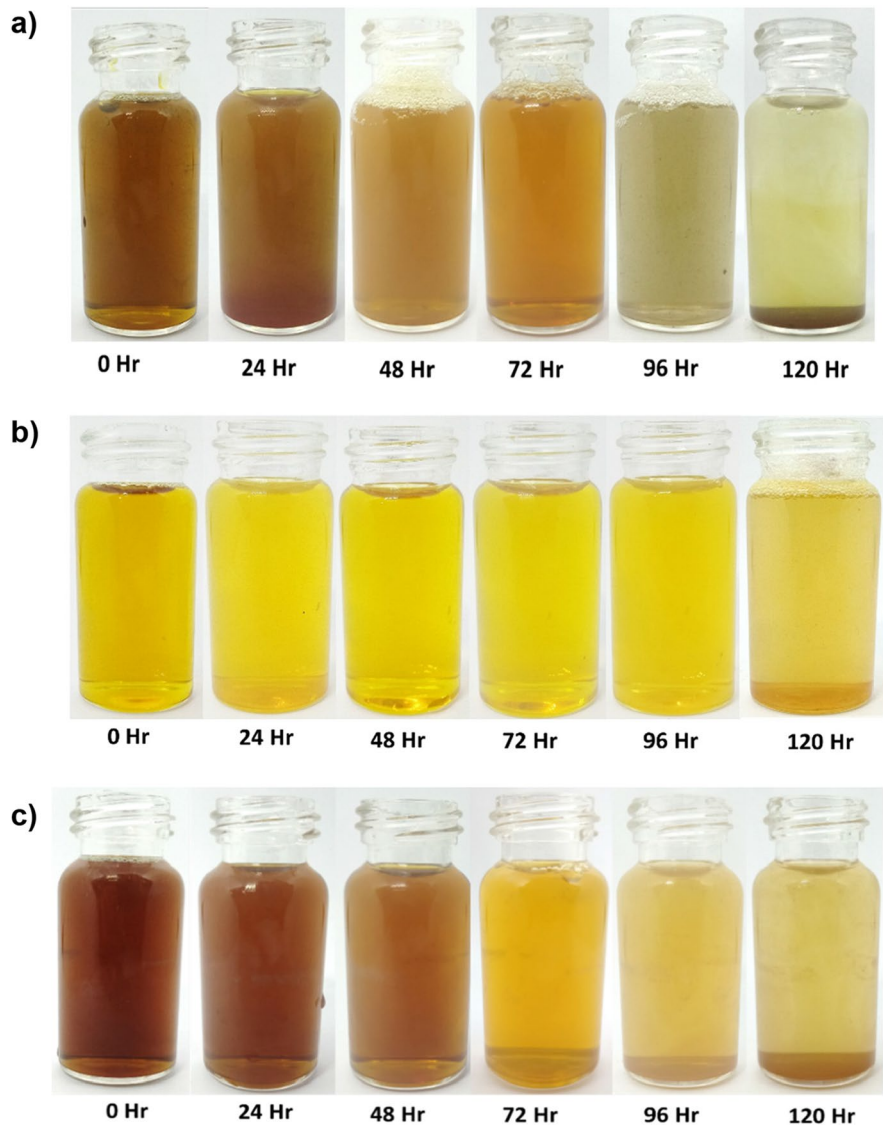

Fig. 9 Images of nanoparticle solution obtained at different time intervals for experiments: **a**) E1 (silver precursor followed by copper precursor), **b**) E2 (copper precursor followed by silver precursor), and **c**) E3 (simultaneous addition of precursors) indicating color change with time for particles obtained in the experiments E1 and E3, whereas no color change for particles obtained in E2

oxidation. High-intensity O 1 s peaks for the nanoparticles synthesized in E1 and E3 indicate higher surface oxidation compared to that seen in nanoparticles synthesized in E2. Therefore, core–shell nanoparticles synthesized in E2 are resistant to oxidation than the particles synthesized in E1 and E3. The analysis of the above results is discussed in the next section.

Discussion

The results discussed in the previous section confirm that different morphologies of bimetallic nanoparticles can be synthesized by changing the operating conditions. In this section, we propose the different pathway mechanisms that lead to the formation of varied nanoparticle structures.

The nanoparticle reduction kinetics is fast owing to a high concentration of reducing agent (ascorbic acid) and microwave heating. Under these conditions, the reaction pathways for nanoparticle formation are governed by the thermodynamics of the system. According to Ferrando et al. (Ferrando et al. 2008), the structure of the bimetallic nanoparticles consisting of two metals (Cu and Ag here) depends on the following three parameters.

Relative strengths of Cu − Cu, Ag–Ag, and Cu-Ag bonds Considering the bond strength in Table 1, the following relationships can be established between different bond strengths: Cu-Cu > Cu-Ag > Ag–Ag. The bond strength determines the thermodynamic stability of the total system and influences the mixing of the metals. Considering a bimetallic nanoparticle-containing copper and silver surface, new copper atoms would preferentially deposit on the copper surface of the particle due to higher Cu-Cu bond strength as compared to Cu-Ag bond strength. Whereas new silver atoms would deposit on the copper surface of the particle rather than the silver surface due to higher Cu-Ag bond strength as compared to Ag–Ag bond strength.

Table 1 The elemental properties of Cu and Ag which determine the structure of bimetallic nanoparticles (Zaleska-Medynska et al. 2016)

	Bond strength (dissociation energy) (kJ/mol)	Surface energy (J/m^2)	Atomic radius (pm)
Copper	190.4 ± 13 (Cu-Cu) 172 ± 8 (Cu-Ag)	1.790	125
Silver	159 ± 8 (Ag–Ag) 172 ± 8 (Ag–Cu)	1.246	144

Surface energies of bulk elements Cu and Ag The element with the lowest surface energy tends to form the surface of a particle. In the case of Ag and Cu, the lower surface energy of Ag favors the formation of the nanoparticles with Ag atoms on the surface (Osowiecki et al. 2018).

Relative atomic sizes The element with a smaller atomic size preferentially forms the core of a particle. In this case, Cu with a smaller size will preferentially form the core of the particle. These parameters for Ag and Cu are listed in Table 1. We use this to understand the mechanism of the formation of different structures in different experimental protocols.

The above physiochemical properties of metals influence the reaction pathways and hence the final nanoparticle structure. We propose the mechanisms for nanoparticle formation under the different experimental conditions taking the aforementioned properties into account.

Experiment E1

Here, the synthesis of nanoparticles can be considered as a reaction in series and can be represented as follows:

$$A + R \xrightarrow{\text{microwave}} A' + R + B \xrightarrow{\text{microwave}} A'B'(\text{Janus}) \quad (R1)$$

where A and B are the precursors and R is the reducing agent. A' and A'B' are the products. Specifically, A here is silver nitrate, B is copper nitrate, and R is ascorbic acid. Initially, when silver nitrate (A) is added to the solution, the silver ions are reduced by ascorbic acid, and silver nanoparticles (A') are formed. Later, when the copper precursor (B) is added to the solution, the reduction of copper ions by ascorbic acid is accelerated by microwave heating. The existing silver nanoparticles act as nucleating sites to the copper atoms. These nucleating sites provide a low energy path for the generation of the copper nucleus via surface deposition and help in the

process of copper nucleation on the silver surface. This leads to partial deposition of a copper layer on the silver nanoparticle surface through heterogeneous nucleation. It was also observed that Ag nanoparticles catalyze the formation of Cu atoms at room temperature (see Supporting Information). This is consistent with the study of Grouchko (Grouchko et al. 2009). Furthermore, when more copper atoms are generated through reduction, the copper layer deposited previously on the silver surface acts as a nucleating site instead of the remnant silver surface. This is attributed to higher Cu-Cu bond strength as compared to Cu-Ag bond strength. Thus, the copper atoms deposit preferentially on the copper layer instead of the silver surface. This inhibits the formation of a copper shell around the silver nanoparticle and results in the formation of AgCu Janus particles, as depicted in Fig. 10. There exists a possibility of Cu atoms entering into the subsurface of Ag nanoparticles, leading to the formation of quasi-Janus structures. In these structures, the copper surface is covered with an Ag monolayer, as reported in the studies performed by Bochicchio et al. and Baletto et al. (Bochicchio and Ferrando 2013; Baletto et al. 2003). However, the formation of quasi-Janus structures could not be confirmed in characterization studies due to the resolution limitations.

Experiment E2

When the reaction sequence is altered in experiment E2, nanoparticle formation can be considered as reactions in series as well and is represented as follows:

$$B + R \xrightarrow{\text{microwave}} B' + R + A \xrightarrow{\text{microwave}} B'A' \text{ (Core} - \text{Shell)} \quad \text{(R2)}$$

Here, the copper precursor (B) is reduced first in the presence of ascorbic acid (R) using microwave heating. The microwave enhances the reduction rate of copper ions. The time required to synthesize copper nanoparticles is drastically reduced from 2–16 h when conventional heating methods are used (Biçer and Şişman 2010; Xiong et al. 2011; Liu et al. 2012) to 1 min in the microwave. Microwaves enhance the rate of chemical reactions by decreasing the activation energy of the reactant molecules (Zhou et al. 2016). This reduces the total reaction time of the copper ions with ascorbic acid resulting in an enhanced rate of copper nanoparticle (B') formation. Furthermore, when silver nitrate (A) was added to the solution, the silver ions undergo rapid reduction following two mechanisms: (i) they are reduced by ascorbic acid and (ii) the silver ions also undergo the galvanic displacement reaction with copper on the particle surface. The reduction potential of copper ($Cu^{2+}/Cu = +0.34$ V) is lower than the silver ($Ag^{+}/Ag = +0.7996$) (Ferrando et al. 2008). Hence, the galvanic displacement reaction occurs wherein copper reduces the silver ions in the solution. As a result, silver preferably deposits on the copper nucleus. This type of growth, along with the factors like bond strength, surface energies, and atomic radius, promotes the formation of copper core and silver shell (Fig. 11). Therefore, when the sequence of the precursor addition is changed, the Cu-Ag core–shell (B'A') formation is favored. It was observed that the particles synthesized in this case have relatively larger polydispersity than the other two cases. This can be attributed to the presence of more than one core in the particles which leads to uneven growth of the silver shell.

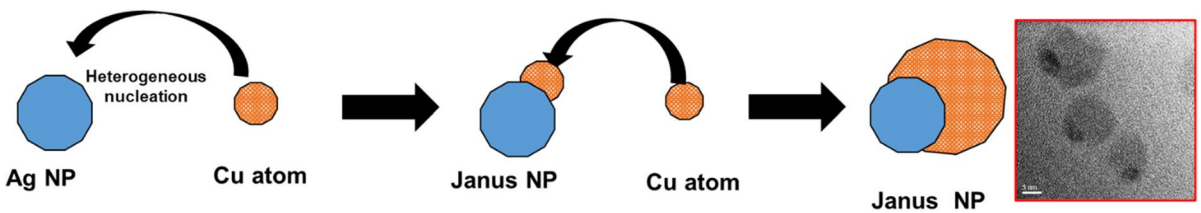

Fig. 10 Schematics describing the proposed mechanism for the formation of Janus Ag–Cu bimetallic nanoparticles synthesized in the experiment E1

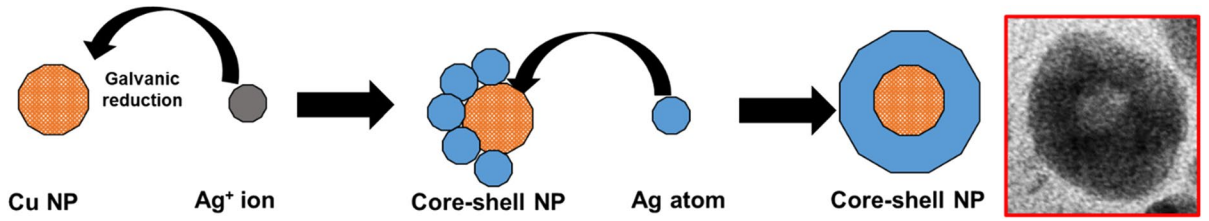

Fig. 11 Schematics describing the proposed mechanism for the formation of Core–shell Cu-Ag bimetallic nanoparticles synthesized in the experiment E2

Experiment E3

In this case, the nanoparticle synthesis is considered as multiple reactions in parallel since both reducing agents are reduced simultaneously. The nanoparticle formation can be represented as

$$A + R \xrightarrow{\text{microwave}} A' \quad \text{(R3.1)}$$

$$B + R \xrightarrow{\text{microwave}} B' \quad \text{(R3.2)}$$

$$A' + B' \longrightarrow A'B' \text{ (Janus)} \quad \text{(R3.3)}$$

Here, copper and silver precursors are mixed simultaneously, and a reducing agent is added to the mixture. The silver ions are reduced instantaneously and form nuclei. Simultaneously, the reduction of copper is initiated, but this reaction rate is slow compared to the reduction rate of silver. This is attributed to the relatively high reduction potential of silver ions ($Ag^{+}/Ag = +0.7996$) than the copper ions ($Cu^{2+}/Cu = +0.34$) (Ferrando et al. 2008). It is hence easier for the silver to undergo a reduction in a weak reducing agent like ascorbic acid. Consequently, a higher number of silver nuclei are formed than copper nuclei in the solution. The copper ions in the solution, as they undergo reduction, will further grow on the formed copper and silver nuclei through homogenous and heterogeneous growth, respectively. Thus, a mixture of Janus-like particles and copper nanoparticles is formed in this case, as depicted in Fig. 12. During simultaneous nucleation, the nanoparticles may form aggregated structures, initially leading to the formation of an intermixed configuration. The high temperature further induces phase separation of copper and silver atoms leading to the formation of Janus or core–shell structure, as explained in the simulation studies performed by Nelli et al. (Nelli and Ferrando 2019). Eventually, the nanoparticles formed in E3 consist of a mixture of Janus, core–shell, and copper nanoparticles.

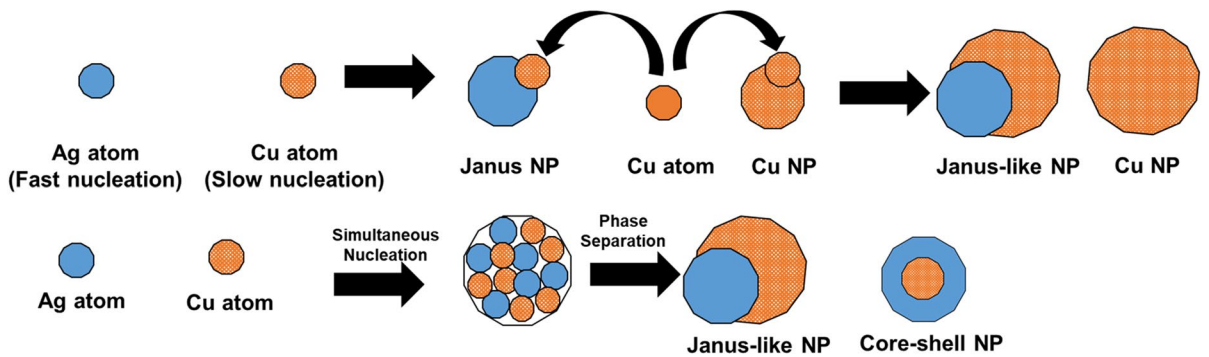

Fig. 12 Schematics describing the proposed mechanism for the formation of a mixture of Janus Ag–Cu bimetallic and copper nanoparticles synthesized in the experiment E3

Anti-oxidation studies

Nanoparticles obtained from the experiments E1 and E3 show weak resistance to oxidation. Janus nanoparticles obtained in the experiments E1 and E3 contain copper at the surface. The copper surface is susceptible to easy oxidation under ambient conditions and results in the degradation of these bimetallic nanoparticles. This manifests as a decrease in LSPR peaks and changes in color, as shown in Figs. 8a and c and 9a and c. The particles obtained in experiment E2 consist of the copper core protected by the silver shell. This prevents the oxidation of copper as it is not exposed, enhancing the stability of the nanoparticles. Hence, the LSPR peak in Fig. 8b is dominant, and no color change in the solution is observed in Fig. 9b.

Conclusions

This work explores the possibility of tuning the nanoparticle structures through different reaction pathways. The pathways were varied by changing the sequence of addition of reactants. In the experiments E1 and E2, nanoparticle synthesis was carried out sequentially through a series of reactions. These experiments emphasized the importance of sequence in the series reactions as two different structures of nanoparticles, viz. Janus and core–shell were obtained for experiments E1 and E2, respectively, whereas experiment E3 showed that a mixture of nanoparticle structures was obtained as the synthesis was carried out in simultaneous parallel reactions. Moreover, it was observed that the microwave enhances the rate of nanoparticle formation in all three experiments. Specifically, the copper nanoparticles were formed faster than conventional heating methods described in the literature.

The anti-oxidation studies of the nanoparticles synthesized showed that core–shell structures were stable and resistant to oxidation compared to the Janus structures. This indicates that an appropriate synthesis method should be chosen based on the application of the nanoparticles.

The study helps us determine the right sequence of precursor addition to obtaining stable bimetallic nanoparticles of different morphologies. The mechanism of formation of different morphology of particles is proposed. It was shown that different structures of nanoparticles could be obtained in the same apparatus by changing only the operating conditions. This allows us to explore different kinetic/reaction pathways to attain different states which may not be thermodynamically favorable.

Supplementary Information The online version contains supplementary material available at https://doi.org/10.1007/s11051-021-05238-w.

Acknowledgements The authors would like to acknowledge the central electron microscopy facility IIT Madras for the TEM and SAED, Department of Chemical Engineering for providing SEM facility. The authors would like to thank Prof. S. Sankaran, Dept. of Metallurgical and Materials Engineering, IIT Madras, for his valuable insights on the XPS and XRD data analysis.

Declarations

Conflict of interest The authors declare that they have no conflict of interest.

References

Al-Sarraj A, Saoud KM, Elmel A et al (2021) Optoelectronic properties of highly porous silver oxide thin film. SN Appl Sci 3:1–13. https://doi.org/10.1007/s42452-020-04091-1

Baletto F, Mottet C, Ferrando R (2003) Growth of three-shell onionlike bimetallic nanoparticles. Phys Rev Lett 90:4. https://doi.org/10.1103/PhysRevLett.90.135504

Biçer M, Şişman I (2010) Controlled synthesis of copper nano/microstructures using ascorbic acid in aqueous CTAB solution. Powder Technol 198:279–284. https://doi.org/10.1016/j.powtec.2009.11.022

Bochicchio D, Ferrando R (2013) Morphological instability of core-shell metallic nanoparticles. Phys Rev B - Condens Matter Mater Phys 87:165435. https://doi.org/10.1103/PhysRevB.87.165435

Cai Y, Piao X, Gao W et al (2017) Large-scale and facile synthesis of silver nanoparticles: via a microwave method for a conductive pen. RSC Adv 7:34041–34048. https://doi.org/10.1039/c7ra05125e

Chen L, Deming CP, Peng Y et al (2016) Gold core@silver semishell Janus nanoparticles prepared by interfacial etching. Nanoscale 8:14565–14572. https://doi.org/10.1039/c6nr03368g

Cheng Y, Samia AC, Li J et al (2010) Delivery and efficacy of a cancer drug as a function of the bond to the gold nanoparticle surface. Langmuir 26:2248–2255. https://doi.org/10.1021/la902390d

Cuenya BR (2010) Synthesis and catalytic properties of metal nanoparticles: size, shape, support, composition, and oxidation state effects. Thin Solid Films 518:3127–3150. https://doi.org/10.1016/j.tsf.2010.01.018

Ferrando R (2015) Symmetry breaking and morphological instabilities in core-shell metallic nanoparticles. J Phys Condens Matter 27:013003

Ferrando R, Jellinek J, Johnston RL (2008) Nanoalloys: from theory to applications of alloy clusters and nanoparticles. Chem Rev 108:845–910. https://doi.org/10.1021/cr040090g

Gawande MB, Goswami A, Asefa T, et al (2016) Cu and Cu-based nanoparticles : synthesis and applications in catalysis. Chem Rev 3722–3811

Grouchko M, Kamyshny A, Ben-Ami K, Magdassi S (2009) Synthesis of copper nanoparticles catalyzed by pre-formed silver nanoparticles. J Nanoparticle Res 11:713–716. https://doi.org/10.1007/s11051-007-9324-5

Horikoshi S, Abe H, Torigoe K, Serpone N (2010) Access to small size distributions of nanoparticles by microwave-assisted synthesis . Formation of Ag nanoparticles in aqueous carboxymethylcellulose solutions in batch and continuous-flow reactors. Nanoscale 1441–1447. https://doi.org/10.1039/c0nr00141d

Horikoshi S, Serpone N (2013) Microwaves in nanoparticle synthesis. Wiley-VCH Verlag GmbH & Co, KGaA, Weinheim

Kushida Y, Saito N, Shigeno M, Yamaguchi M (2017) Multiple competing pathways for chemical reaction: drastic reaction shortcut for the self-catalytic double-helix formation of helicene oligomers. Chem Sci 8:1414–1421. https://doi.org/10.1039/c6sc01893a

Langlois C, Li ZL, Yuan J et al (2012) Transition from core-shell to Janus chemical configuration for bimetallic nanoparticles. Nanoscale 4:3381–3388. https://doi.org/10.1039/c2nr11954d

Liu QM, Yasunami T, Kuruda K, Okido M (2012) Preparation of Cu nanoparticles with ascorbic acid by aqueous solution reduction method. Trans Nonferrous Met Soc China 22:2198–2203. https://doi.org/10.1016/S1003-6326(11)61449-0

Lu L, Wang H, Zhou Y et al (2002) Seed-mediated growth of large, monodisperse core-shell gold-silver nanoparticles with Ag-like optical properties. Chem Commun 2:144–145. https://doi.org/10.1039/b108473a

Ma Y, Li W, Cho EC et al (2010) Au@Ag core-shell nanocubes with finely tuned and well-controlled sizes, shell thicknesses, and optical properties. ACS Nano 4:6725–6734. https://doi.org/10.1021/nn102237c

Mandal S, Selvakannan PR, Pasricha R, Sastry M (2003) Keggin ions as UV-switchable reducing agents in the synthesis of Au core-Ag shell nanoparticles. J Am Chem Soc 125:8440–8441. https://doi.org/10.1021/ja034972t

McIntyre NS, Cook MG (1975) X-ray photoelectron studies on some oxides and hydroxides of cobalt, nickel, and copper. Anal Chem 47:2208–2213. https://doi.org/10.1021/ac60363a034

Miyakawa M, Hiyoshi N, Nishioka M et al (2014) Continuous syntheses of Pd@Pt and Cu@Ag core-shell nanoparticles using microwave-assisted core particle formation coupled with galvanic metal displacement. Nanoscale 6:8720–8725. https://doi.org/10.1039/c4nr00118d

Nadagouda MN, Varma RS, Nanostructures CS (2007) A greener synthesis of core (Fe, Cu) -Shell (Au, Pt, Pd, and Ag) nanocrystals using aqueous vitamin C & DESIGN. Cryst Growth Des 7:2582–2587

Nelli D, Ferrando R (2019) Core-shell vs. multi-shell formation in nanoalloy evolution from disordered configurations. Nanoscale 11:13040–13050. https://doi.org/10.1039/c9nr02963j

Ney JE, Wolfe JP (2005) Selective synthesis of 5- or 6-aryl octahydrocyclopenta[b]pyrroles from a common precursor through control of competing pathways in a Pd-catalyzed reaction. J Am Chem Soc 127:8644–8651. https://doi.org/10.1021/ja0430346

Osowiecki WT, Ye X, Satish P et al (2018) Tailoring morphology of Cu–Ag nanocrescents and core–shell nanocrystals guided by a thermodynamic model. J Am Chem Soc 140:8569–8577. https://doi.org/10.1021/jacs.8b04558

Panigrahi S, Kundu S, Ghosh SK et al (2005) Sugar assisted evolution of mono- and bimetallic nanoparticles. Colloids Surf A Physicochem Eng Asp 264:133–138. https://doi.org/10.1016/j.colsurfa.2005.04.017

Pacioni NL, Filippenko V, Presseau N, Scaiano JC (2013) Oxidation of copper nanoparticles in water: mechanistic insights revealed by oxygen uptake and spectroscopic methods. Dalt Trans 5832–5838. https://doi.org/10.1039/c3dt32836h

Pellarin M, Issa I, Langlois C et al (2015) Plasmon spectroscopy and chemical structure of small bimetallic Cu(1–x) Agxclusters. J Phys Chem C 119:5002–5012. https://doi.org/10.1021/jp511671m

Rossi G, Rapallo A, Mottet C et al (2004) Magic polyicosahedral core-shell clusters. Phys Rev Lett 93:1–4. https://doi.org/10.1103/PhysRevLett.93.105503

Schanche J (2003) Microwave synthesis solutions from Personal Chemistry. Mol Divers 7(2–4):293–300

Song Y, Liu K, Chen S (2012) AgAu bimetallic janus nanoparticles and their electrocatalytic activity for oxygen reduction in alkaline media. Langmuir 28:17143–17152. https://doi.org/10.1021/la303513x

Tsuji M, Hikino S, Sano Y, Horigome M (2009) Preparation of Cu@Ag core–shell nanoparticles using a two-step polyol process under bubbling of N2 gas Masaharu. Chem Lett 38:518–519. https://doi.org/10.1246/cl.2009.518

Tsuji M, Hikino S, Tanabe R et al (2010) Syntheses of Ag/Cu alloy and Ag/Cu alloy core Cu shell nanoparticles using a polyol method. Cryst Eng Comm 12:3900. https://doi.org/10.1039/c0ce00064g

Valodkar M, Modi S, Pal A, Thakore S (2011) Synthesis and anti-bacterial activity of Cu, Ag and Cu-Ag alloy nanoparticles: a green approach. Mater Res Bull 46:384–389. https://doi.org/10.1016/j.materresbull.2010.12.001

Wang R, Yao Y, Shen M, Wang X (2016) Green synthesis of AuatAg nanostructures through a seed-mediated method and their application in SERS. Colloids Surf A Physicochem Eng Asp 492:263–272. https://doi.org/10.1016/j.colsurfa.2015.11.076

Xiong J, Wang Y, Xue Q, Wu X (2011) Synthesis of highly stable dispersions of nanosized copper particles using l-ascorbic acid. Green Chem 13:900–904. https://doi.org/10.1039/c0gc00772b

Yabuki A, Tanaka S (2011) Oxidation behavior of copper nanoparticles at low temperature. Mater Res Bull 46:2323–2327. https://doi.org/10.1016/j.materresbull.2011.08.043

Zaleska-Medynska A, Marchelek M, Diak M, Grabowska E (2016) Noble metal-based bimetallic nanoparticles: the effect of the structure on the optical, catalytic and photocatalytic properties. Adv Colloid Interface Sci 229:80–107. https://doi.org/10.1016/j.cis.2015.12.008

Zhang W, Li Y, Niu J, Chen Y (2013) Photogeneration of reactive oxygen species on uncoated silver, gold, nickel, and silicon nanoparticles and their anti-bacterial effects. Langmuir 29:4647–4651. https://doi.org/10.1021/la400500t

Zhou J, Xu W, You Z et al (2016) A new type of power energy for accelerating chemical reactions: the nature of a microwave-driving force for accelerating chemical reactions. Sci Rep 6:25149. https://doi.org/10.1038/srep25149